LONGITUDINAL BUNCHED-BEAM INSTABILITIES IN A BARRIER RF SYSTEM

Y. H. Chin and H. Tsutsui, KEK, 1-1 Oho, Tsukuba-shi, Ibaraki-ken, 305, Japan

Abstract

This paper deals with theoretical and numerical analysis of longitudinal instabilities in a barrier RF system. A theory was developed to formulate using the Vlasov equation and the synchrotron- energy mode expansion. The result can be expressed in a form of eigenvalue matrix. A simulation code ECLIPS (Evaluation Code for Longitudinal Instabilities in a Proton Synchrotron) was also developed. Both were applied to the JHF 50GeV proton synchrotron at injection. They show excellent agreements. The results demonstrate that the microwave and the negative mass instabilities in a bunched beam can be explained by mode-coupling instabilities.

1 INTRODUCTION

The barrier RF system[1] has been proposed as a new method to achieve a high beam current by creating a very flat bunched beam. Unlike in a conventional RF system, particles are drifting freely between two discreet single-turn RF waveforms at which they suddenly receive repelling forces to turn around. The particle trajectory results in an squarish shape in the phase space. The bunch length can be easily controlled by changing the distance between two barriers. The synchrotron motion tends to become very slow (of the order of 10 Hz at the JHF[2]), while its frequency spread becomes comparable to the synchrotron frequency itself. An idea of higher harmonic cavity is aimed to create a similar RF environment[3].

The collective stability of the beam due to wake fields in a barrier RF system may resemble that in a coasting beam, provided that the wave length of the beam density modulation is shorter than the bunch length and the instability growth is much faster than the synchrotron oscillation. Such a coasting beam approximation has beam made for years to allow the usage of the Keil-Schnell-Boussard criterion to a long proton bunch. It is, however, not clear what should replace the Keil-Schnell-Boussard criterion when the coasting beam approximation is inappropriate in a bunched-beam.

A more direct approach, based on the bunched-beam mode expansion of the phase space density, has been proposed by Sacherer[4]. This is an attempt to explain the microwave and negative mass instabilities in a bunched beam in terms of couplings between different synchrotron modes. The mode-coupling offers a possible explanation for existence of the threshold. However, his formalism lacks the Landau damping effect due to a synchrotron frequency spread (or energy spread), which plays an essential role in a coasting beam to set the threshold. Therefore, his mode-coupling theory fails to make a transition to the coasting beam theory.

Our goal is to construct a theory proper bunched-beam longitudinal instabilities in a barrier RF system with the Landau damping effect included and without the coasting beam approximation. The correct treatment of the synchrotron frequency spread in the squarish barrier bucket can be done by describing the synchrotron motion using action-angle variables[5]. From numerical comparisons between the theory and simulations, we can show that the coasting beam instabilities are indeed transformed to mode-coupling instability in a long bunch.

2 VLASOV ANALYSIS

In this section, we briefly outline the formalism. The phase space particle trajectory in the barrier bucket is illustrated in Fig. 1:

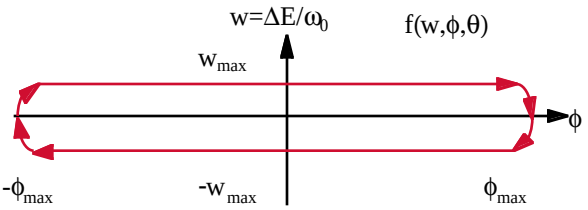

Figure 1: Phase space trajectory in a barrier bucket.

where ΔE is the energy deviation from the average energy E_0, ω_0 is the revolution frequency, and ϕ is the relative position of particle in a bunch in angle. We use θ, the angular position of particle in a ring, as an independent variable. Let us approximate this trajectory by a square for simplicity. The constant of motion (action I) is the area confined by the square trajectory:

$$I = \frac{1}{2\pi}\int dw d\phi = \frac{2}{\pi}\phi_{\max} w_{\max} \tag{1}$$

The corresponding angle variable is the phase of the particle oscillation around the trajectory:

$$\psi \equiv \omega_s t = -\frac{\eta}{\beta^2}\cdot\frac{\pi\omega_0^2}{2\phi_{\max}E_0}\cdot w_{\max} t \tag{2}$$

where η is the slippage factor, βc is particle velocity and

$$\omega_s \equiv \nu_s(I)\omega_0 = -\frac{\eta}{\beta^2}\cdot\frac{\omega_0^2}{E_0}\left(\frac{\pi}{2\phi_{\max}}\right)^2 I \tag{3}$$

is the synchrotron frequency proportional to I.

The evolution of phase space distribution $f(I,\psi,\theta)$ obeys the Vlasov equation:

$$\frac{\partial f}{\partial\theta} + \psi'\frac{\partial f}{\partial\psi} + I'\frac{\partial f}{\partial I} = 0 \tag{4}$$

where a prime means taking the derivative with respect

0-7803-4376-X/98/$10.00 © 1998 IEEE

to θ. We solve the above equation by the perturbation technique. Since I and ψ are the canonical variables, the perturbed part of $f(I,\psi,\theta)$ can be factorized to separate functions for each of them. The angle dependent function can be Fourier expanded due to the periodicity with period 2π. The phase space distribution can be thus written as

$$f(I,\psi,\theta) = f_0(I) + \sum_{m=-\infty}^{\infty} f_m(I)\exp(im\psi)\exp(-i\Omega\theta) \qquad (5)$$

Here, the integer m stands for synchrotron mode number. The line charge density $\rho(\phi)$ corresponding to the perturbed part of the phase space distribution is given by

$$\rho(\phi) = \frac{2}{\frac{2}{\pi}\phi_{\max}} \cdot \sum_{m=-\infty}^{\infty} \begin{bmatrix} i\sin(m\frac{\phi}{\phi_{\max}}\frac{\pi}{2}) \\ \cos(m\frac{\phi}{\phi_{\max}}\frac{\pi}{2}) \end{bmatrix} \cdot \int_0^{\infty} f_m(I)dI \qquad (6)$$

The upper and lower terms in the bracket correspond to odd and even integers of m, respectively. Figure 2 shows $\rho(\phi)$ for the lowest three synchrotron modes.

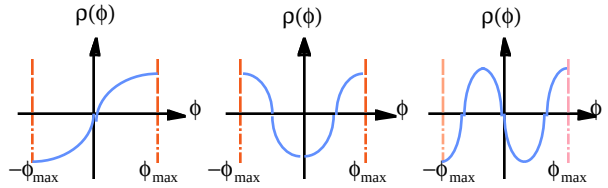

Figure: 2 The line charge density $\rho(\phi)$ for m=1 (dipole), m=2 (quadrupole) and m=3 (sextupole) modes.

Using the impedance $Z(\omega/\omega_0)$ and the Fourier transform of $\rho(\phi)$, $\tilde{\rho}(\nu)$, we can write

$$I' = -e^2 N \frac{\phi_{\max}}{\pi^2}\mathrm{sgn}(w)\sum_{p=-\infty}^{\infty} Z(p+\Omega)\tilde{\rho}(p+\Omega) \times \exp(-i(p+\Omega)\phi - i\Omega\theta) \qquad (7)$$

$$\psi' = \nu_s(I) \qquad (8)$$

where N is the number of particles in a bunch. Substitution of Eqs. (5), (7) and (8) into Eq. (4) yields an integral equation for $f_m(I)$:

$$(\Omega - m\nu_s(I))f_m(I) = i\frac{2eI_b m}{\pi^3\omega_0}\sum_{n=-\infty}^{\infty}\frac{df_0(I)}{dI}i^{n-m}\int_0^{\infty} f_n(I')dI' \times \sum_{p=-\infty}^{\infty}\frac{Z(p+\Omega)}{p+\Omega}C_m^*(p+\Omega)C_n(p+\Omega) \qquad (9)$$

where I_b is the circulating current and

$$C_m(q) = \frac{q\frac{2}{\pi}\phi_{\max}\begin{bmatrix} i\cos(q\phi_{\max}) \\ \sin(q\phi_{\max}) \end{bmatrix}}{m^2 - \left(q\frac{2}{\pi}\phi_{\max}\right)^2} \qquad (10)$$

The same rule as in Eq. (6) is applied to Eq. (10).

Let us solve Eq. (9) by expanding the unknown function $f_m(I)$ using a complete set of orthogonal polynomials The choice of appropriate polynomials depends on the unperturbed distribution $f_0(I)$ (the initial energy distribution). For a Gaussian distribution, it is the Laguerre polynomials. After lengthy calculation, Eq. (9) transforms to a matrix eigenvalue equation for Ω and an expansion coefficient vector $\mathbf{a}$:

$$\Omega\mathbf{I}\cdot\mathbf{a} - \mathbf{N}\cdot\mathbf{a} = \mathbf{M}\cdot\mathbf{a} \qquad (11)$$

where $\mathbf{I}$ is the unit matrix and the elements of other matrixes are explicitly given by

$$N_{nl}^{mk} = -m\frac{\pi\eta}{\sqrt{2}\phi_{\max}\beta^2}\left(\frac{\Delta E}{E_0}\right)_{rms}\delta_{mn}L_{kl} \qquad (12)$$

$$L_{kl} = \int_0^{\infty}\sqrt{x}e^{-x}L_k(x)L_l(x)dx \qquad (13)$$

$$M_{nl}^{mk} = -im\frac{\sqrt{2}I_b}{\pi^{5/2}\phi_{\max}(\Delta E/E_0)_{rms}E_0/e}i^{n-m}\delta_{k0}\delta_{l0} \times \sum_{p=-\infty}^{\infty}\frac{Z(p+\Omega)}{p+\Omega}C_m^*(p+\Omega)C_n(p+\Omega) \qquad (14)$$

Here, $L_k(x)$ is the Laguerre polynomials.

3 NUMERICAL EXAMPLES

Table 1 summaries the main parameters of JHF 50 GeV proton synchrotron at injection. The resonator model is used to characterize the impedance of the ring.

Table 1: Main parameters of JHF 50 GeV ring.

Injection energy, E_I	3 GeV
Circumference, C	1442 m
Design circulating current, I_b	6.65 A
Slippage factor, η	-0.05
Half bunch length in angle, $\phi_{\max}$	150 degree
RMS energy spread, $(\Delta E/E_0)_{rms}$	0.212%
RMS synchrotron frequency, $\Omega_0/2\pi$	16.96 Hz
Impedance of the ring at peak, R_s	10 kΩ
Resonant frequency, f_r	3.4 MHz
Q-value	1

Figure 3 shows the coherent synchrotron mode frequencies (normalized by Ω_0) and the growth rate as a function of the circulating current. Several modes start to couple at about 5A, signaling the onset of instabilities. Figure 4 shows the time evolution of the rms energy spread at 5A for various initial energy spread. One can see that the energy distribution stops to blow up when the initial energy spread is about 0.2%, in a good agreement with the analytical result (a slow increase of the energy spread attributes to non-compensation of the energy loss due to wake fields in simulations). Though not shown here, the phase space plot shows an uniform particle density after a blow-up of the energy spread. This is a signature of the microwave instability. The 5A threshold for circulating current is lower than the design value of 6.65A, which suggests a need of reducing the impedance.

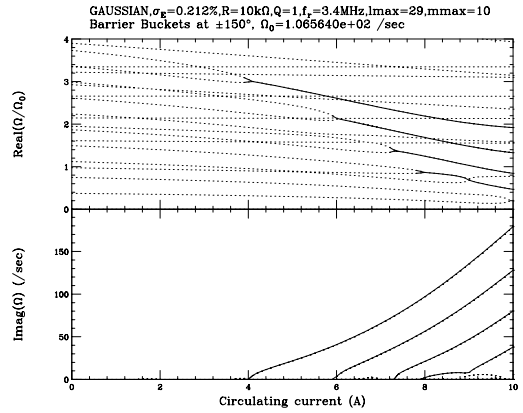

Figure 3: Coherent synchrotron mode frequencies and the growth rate versus the circulating current (theory).

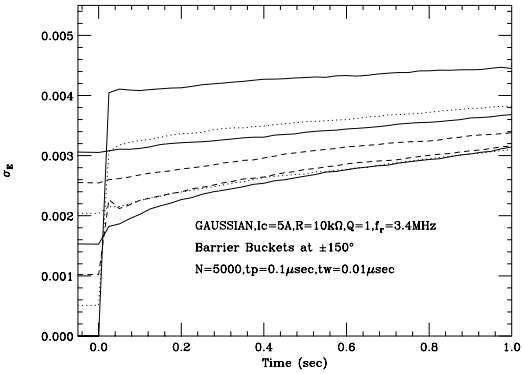

Figure 4: Time evolution of the rms energy spread for various initial spread (simulations).

Next, let us apply to a pure inductive impedance. The inductance is chosen to be equal to that of the resonator model at low frequency. The coasting beam theory predicts the excitation of negative mass instability. Figure 5 shows the coherent synchrotron mode frequencies and the growth rate versus the circulating current. Many synchrotron modes couple simultaneously with their negative mode partners (they are mirror images with respect to the Ω=0 line) at about 9A. The growth rate increases very rapidly after the mode-couplings. Figure 6 shows the time evolution of the rms energy spread at 9A for various initial energy spread. The threshold of energy spread appears to be around 0.21%, in a good agreement with the analytical result again. Figure 7 shows the phase space distribution after the instability ceased for the initial energy spread of 0.05%. Strong concentration of particles can be observed at several places as expected for the negative mass instability. According to the coasting beam theory, the negative mass instability has the same threshold for all coasting beam modes "n" for a pure inductive impedance. This behavior agrees with the simultaneous onset of mode-coupling instabilities of all synchrotron modes as seen in Fig. 5. Another important point is that the real part of mode frequencies vanishes after mode-couplings. Namely, the modes stop moving in phase space, while they grow. This behavior corresponds to the characteristic of the negative mass instability that the crests of beam density are fixed in the beam frame.

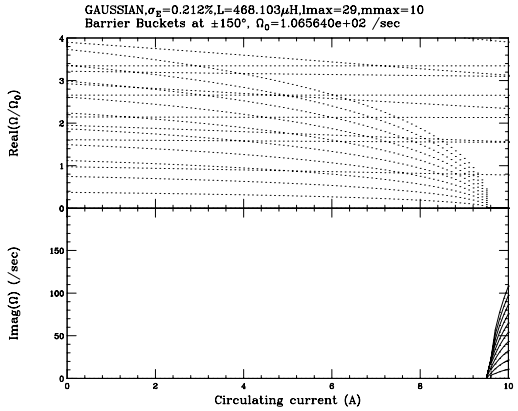

Figure 5: Coherent synchrotron mode frequencies and the growth rate for the inductive impedance (theory).

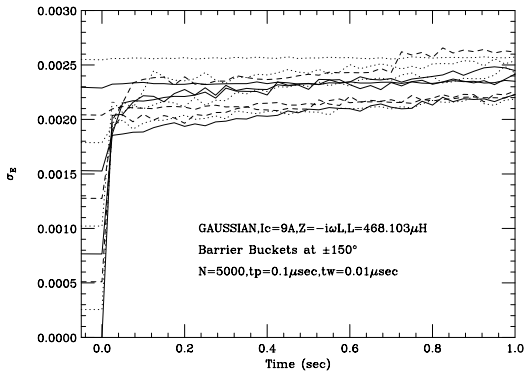

Figure 6: Time evolution of the rms energy spread for various initial spread for the inductive impedance (simulations).

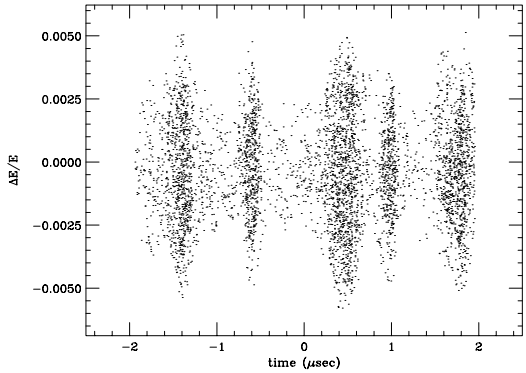

Figure 7: The phase space distribution after the instability ceased for the initial energy spread of 0.05% (simulations).

REFERENCES

[1] J.E. Griffin et. al., IEEE Trans. NS-30, 3502 (1983).
[2] KEK Report JHP-30 (1996).
[3] A. Hofmann and S. Myers, LEP Lote 158 (1979).
[4] F. Sacherer, IEEE Trans. NS-24, 1393 (1977).
[5] Y.H. Chin, Nucl. Instr. Methods, 215, 501 (1983).